NATURAL SCIENCE REVIEW 3 200706 (2026)
nsr.jinr.int

Controlled immobilization of silver nanoparticles on track-etched membranes

I. N. Fadeikina*[1,2], E. V. Andreev[1], O. V. Kristavchuk[1], O. L. Orelovich[1], and P. Yu. Apel[1]

[1] *Joint Institute for Nuclear Research, 141980, Dubna, Russia*
[2] *Dubna State University, Dubna, Russia*

Abstract

The study of the interaction of colloidal solution components with microfiltration membranes is of continuing interest, both in the development of composite porous materials and in the numerous applications of membranes for separating suspensions. This study investigates the transport of silver nanoparticles through track-etched membranes under conditions where the nanoparticles and the membrane surface possess opposite charges. The objective was to establish patterns of nanoparticle deposition based on the membranes structural parameters and the solution flow rate.

A simple criterion was derived to determine nanoparticle retention efficiency by considering convection and diffusion within the pores. This criterion was tested through experiments using polyethylene terephthalate track-etched membranes with pore diameters ranging from 0.1 to 7.1 μm, while the average nanoparticle diameter was 24 nm. By varying the pressure drop, the flow rate of the colloidal solution through the membrane pores was varied.

Nanoparticle retention efficiency was determined using optical spectroscopy and energy-dispersive X-ray analysis. The distribution of nanoparticles on the membrane surface was examined using scanning electron microscopy. It was found that the proposed criterion satisfactorily predicts the transition from nearly complete particle retention to complete transmission when key parameters — pore diameter, membrane thickness, and pressure drop — are varied.

The obtained results provide insights into the controlled immobilization of nanoparticles on membrane surface, which is essential for creating functional nanocomposite devices, such as sensors.

Keywords: track-etched membranes, silver nanoparticles, filtration, nanoparticle immobilization, surface charge, convection, diffusion

DOI: 10.54546/NaturalSciRev.200706

1. Introduction

Composite nanostructured materials play a significant role in materials science and advanced technologies. Immobilization of nanoparticles (NPs) on a surface or in volume is one of the methods used to create membranes with specific functional properties [1–3]. NPs, such as

*Corresponding author e-mail address: i.fadeikina@yandex.ru

Received: 24 March 2026; Revised: 19 May 2026; Accepted: 4 June 2026; Published: 18 June 2026

those of noble metals, are widely used in various fields of science, medicine, and engineering due to their unique physicochemical and optical properties as well as the diverse methods available for their production [4, 5]. A current area of research focuses on the synthesis and study of silver and gold NPs for sensors based on surface-enhanced Raman scattering (SERS). There is a broad range of SERS-based sensor structures, one of which involves dispersing nanoparticles on the surface of a porous membrane. This design allows the device to perform multiple functions — enrichment, separation, and SERS detection [6]. Track-etched membranes, when used as porous substrates, enable the creation of multifunctional sensor with well-defined transport and retention characteristics [7–9].

Analytical techniques are the most traditional applications of track-etched membranes [10]. These membranes have proven indispensable in environmental and biological studies, particularly for capturing, separating, and enumerating aerosol particles, cells, or bacteria [11, 12]. Over the past two decades, many new ideas have emerged regarding the additional functions that track-etched micro- and nanopores can fulfill particularly in the field of sensors [13]. Notable examples include multi-pore amperometric sensors [14], single-pore resistive-pulse sensors [15], and those based on molecular recognition [16]. These new capabilities have been made possible by the development of asymmetrical track-etched nanopores [17].

When fabricating a multifunctional SERS sensor based on the track-etched membrane, NPs can be immobilized directly during synthesis by placing the membrane in the reaction medium [6, 7]. Alternatively, vacuum deposition can be employed [9]. Another possible approach involves depositing nanoparticles onto the surface from a colloidal silver solution [8].

However, passive deposition of NPs on the surface of track-etched membranes can take tens of hours and typically requires agitation of the solution [8]. The slow sorption rate is due to the low concentration of NPs, typically 1–2 mg/L [8]. Additionally, achieving uniform nanoparticle deposition across the entire membrane surface is challenging, and the lengthy process is problematic due to the solutions limited stability. Therefore, there is a topical problem to develop a rapid and effective method for immobilizing nanoparticles on the surfaces of track-etched membranes.

This study aimed to develop a method for the controlled deposition of NPs onto the surface of a track-etched membrane via filtration of a colloidal silver solution. The resulting composite material has potential applications as a sensor, and therefore, the method should be effective for track-etched membranes with various pore diameters.

The patterns of nanoparticle retention by track-etched membranes have been experimentally and theoretically studied in a number of papers [18–28]. When the pore and particle diameters are comparable, sieving is the primary retention mechanism [19, 22]. Conversely, when the pore diameters are significantly larger than the nanoparticle diameters, the membrane can retain nanoparticles by adsorption. Nanoparticle diffusion to the surface becomes a crucial factor [21, 23, 25, 28]. Van der Waals interactions can retain a certain proportion of particles, while the majority of NPs pass through the membrane [21–24, 27]. If the membrane surface and the particle carry the same sign of electric charge, the probability of attractive interaction is very low. Therefore, to ensure that NPs bind effectively to the surface, it is necessary to create opposite charges on the track-etched membranes and the particles [8, 29, 30].

Particles can be retained on both the front surface of the membrane and the pore walls. The particle distribution pattern in the membrane depth can be analyzed using optical methods [20, 25] or electron microscopy [31]. The retention efficiency depends on the flow rate of the solution through the membrane, since the probability of capturing a Brownian nanoparticle decreases due to a reduced residence time inside the pore [27, 28]. Large particles may

be retained on the membrane by an inertial mechanism, which results in increased retention efficiency at higher flow rates [32].

Thus, developing a method for depositing nanoparticles onto a membrane requires careful consideration of all the above factors. The spatial distribution of NPs is a key parameter for various practical applications [33, 34, 47], and therefore, the method should ensure a specific surface density of particles and their appropriate distribution across the membrane surface.

2. Filtration model

The process of depositing particles from a separated mixture onto a porous surface has long attracted researchers' attention. For example, membrane fouling during filtration of protein solutions has been the subject of theoretical analysis and experimental studies [35–38]. These studies primarily focus on the relationship between decreased flow rate and the mechanisms of pore clogging by protein macromolecules and their aggregates.

A number of studies examine in detail the interaction between solid particles and the membrane surface at the pore entrance [39–42]. While these studies are informative in many respects, they are not entirely applicable to the filtration of a colloidal silver solutions through track-etched membranes with pore radii significantly larger than the particles radii. In particular, articles [39, 40] are devoted to the analysis of the transport of micrometer-sized particles, for which the authors neglect the role of Brownian motion. In micro- and ultrafiltration, it is generally assumed that the particle and the membrane surface have the same sign of electric charge [21, 23, 24, 41, 42]. The article [28] provides a detailed treatment of Brownian motion and diffusion in filtration; however, the mathematical model presented is challenging to apply in practice due to the uncertainty surrounding many input parameters.

Let us consider the case where NPs are small enough that Brownian motion near the surface and inside the pores must be accounted for. Track-etched membranes, characterized by an array of cylindrical pores, serve as a suitable model for this process. The surfaces of these track-etched membranes are intentionally modified to provide electric charges of opposite sign to those on the nanoparticles. Under these conditions, a straightforward model can be proposed that accounts for two particle transport mechanisms: convection and diffusion (Figure 1).

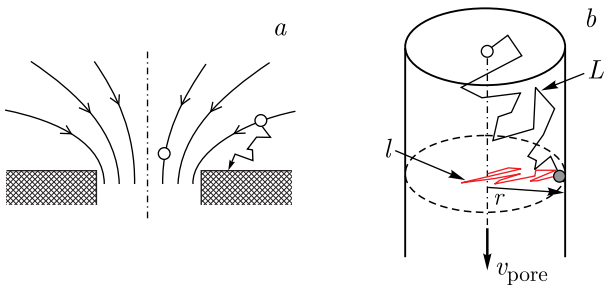

Figure 1. Movement of components of a colloidal solution at the entrance to a track-etched membrane pore (a). Schematic diagram of nanoparticle movement in a membrane pore. The solution moves with an average velocity v_{pore}. L is the particle trajectory due to convective transport and Brownian motion. l is the projection of the trajectory onto the pore cross-section. r is the radial displacement of the particle, equal to the pore radius (b).

Figure 1, a provides a qualitative picture of the motion of NPs at the entrance of a track-etched membrane pore. The convective flow of the liquid layers is shown by smooth lines representing hyperbolic trajectories [43]. NPs carried by this flow into the pore far from the edge of the hole are highly likely to enter the pore and continue moving along its channel. In

addition to convective transport, NPs undergo Brownian motion. One possible trajectory of the stochastic movement of NPs moving near the edge of the hole is shown by the broken line in Figure 1, *b*. NPs are captured by the surface close to the entrance of the hole. Since NPs and the surface carry opposite charges, electrostatic interaction ensures the immobilization of NPs. In other words, we assume that the sticking coefficient is 1.

At a solution ionic strength of 10^{-4} mol/L, the Debye length is $\sim$ 30 nm [44]. Therefore, the influence of the electric field manifests itself when a nanoparticle approaches the surface at a distance comparable to its size. At greater distances, electromigration should not have a significant effect on the movement of NPs.

Let us consider the motion of the nanoparticles that have entered the pore. The average flow velocity v_{pore} through a pore channel of radius r is found from the Poiseuille's law as follows:

$$v_{\text{pore}} = \frac{r^2 \Delta P}{8 \mu l_m}, \tag{1}$$

where ΔP is the pressure drop, μ is the dynamic viscosity coefficient, and l_m is the membrane thickness. The average diffusion time τ_D for a particle to travel a distance equal to the pore radius r [45] is

$$\tau_D = r^2/4D, \tag{2}$$

where D is the diffusion coefficient of NPs, $D = 2 \cdot 10^{-11}$ m$^2 \cdot$s^{-1} for particles with a diameter of 20 nm [46].

The time τ_m required for NPs to pass through the entire length of the pore channel in the membrane is calculated as

$$\tau_m = l_m / v_{\text{pore}} = \frac{8 \mu l_m^2}{r^2 \Delta P}. \tag{3}$$

This time can be considered as the characteristic residence time of a nanoparticle within the pore channel. The ratio of the nanoparticle diffusion time to the residence time in the pore is defined as follows:

$$\tau_D / \tau_m = \frac{r^4 \Delta P}{32 D \mu l_m^2}. \tag{4}$$

Based on this model, the probability of nanoparticle retention by the membrane can be qualitatively predicted. If $\tau_D/\tau_m \gg 1$, NPs pass through the membrane. Conversely, if $\tau_D/\tau_m \ll 1$, NPs are retained by the membrane, mostly accumulating on the frontal surface and near the pore entrance. In the range of $\tau_D/\tau_m \sim 1$, NPs partially pass through while also being retained, resulting in their distribution over the frontal surface and the pore walls of the track-etched membrane.

The ratio τ_D/τ_m can be represented as a dimensionless retention criterion

$$\text{ƥ} = \frac{r^4 \Delta P}{32 D \mu l_m^2}, \tag{5}$$

which allows us to predict the degree of particle retention and select the appropriate filtration mode. Table 1 shows the calculated ƥ-criterion values for track-etched membranes with different pore diameters and three different pressures.

Based on the ƥ-criterion values presented in Table 1, it can be assumed that NPs will be almost completely retained by a membrane with a small pore size (0.1 μm) over the entire range of pressures considered.

Table 1. Calculated values of the retention criterion for several hypothetical track membranes with different pore diameters and thicknesses.

Pore diameter, μm	Thickness, μm	$\frac{r^4\Delta P}{32D\mu l_m^2}$					
		$\Delta P = 0.02$ bar	$\Delta P = 0.4$ bar	$\Delta P = 0.8$ bar	$\Delta P = 1.2$ bar	$\Delta P = 1.6$ bar	$\Delta P = 2.0$ bar
0.10	12	$1.4 \cdot 10^{-4}$	$2.7 \cdot 10^{-3}$	$5.4 \cdot 10^{-3}$	$8.1 \cdot 10^{-3}$	$1.1 \cdot 10^{-2}$	$1.4 \cdot 10^{-2}$
0.40	19	$1.4 \cdot 10^{-2}$	0.28	0.55	0.83	1.1	1.4
0.50	12	$8.4 \cdot 10^{-2}$	1.7	3.4	5.1	6.8	8.4
1.0	23	0.37	7.4	15	22	29	$1.4 \cdot 10^{2}$
7.0	17	$1.6 \cdot 10^{3}$	$3.2 \cdot 10^{4}$	$6.5 \cdot 10^{4}$	$9.7 \cdot 10^{4}$	$1.3 \cdot 10^{5}$	$1.6 \cdot 10^{5}$

Track-etched membranes with pore diameters of 0.4, 0.5, and 1.0 μm have $\hat{\rho}$-criterion values close to 1. Therefore, it is expected that the applied pressure will significantly affect the distribution of NPs across the surface and within pore channels. In contrast, in case of track-etched membrane with a pore diameter of 7.0 μm, the criterion values indicate a short interaction time between NPs and the membrane surface. As a result, the probability of nanoparticle retention on this membrane is low.

3. Materials and methods

3.1. Reagents

The following substances were used: potassium chloride (KCl, > 99%, Sigma-Aldrich), branched polyethyleneimine (PEI) (Mr = 60,000 Da, 50% aqueous solution, Acros), glutaraldehyde (GA) (25% aqueous solution, PanReac), and tableted phosphate-buffered saline (Sigma-Aldrich). Isopropanol (99.9%, Sigma-Aldrich) was used to clean the track-etched membranes. Deionized water with a resistivity of 18 M$\Omega \cdot$cm at 22°C (Milli-Q, Millipore) was used to prepare all solutions.

3.2. Track-etched membranes and their modification

Polyethylene terephthalate (PET, Hostaphan Mitsubishi Polyester Film) track-etched membranes were manufactured at the Flerov Laboratory of Nuclear Reactions (FLNR) of the Joint Institute for Nuclear Research (Dubna) using the technology described in [12]. These PET membranes exhibit identical surface morphology on both sides [12]. Table 2 presents the main structural characteristics of the track membranes used.

Track-etched membranes in the form of disks with a diameter of 4.5 cm were washed with isopropanol and then placed on a shaker in 100 ml of a 0.1% PEI solution for 2 h at room temperature. The PEI solution had a pH of 8.0, which facilitated electrostatic adsorption of the positively charged polyelectrolyte onto the negatively charged membrane surface. To stabilize the modifier layer, the polyethyleneimine molecules were cross-linked with glutaraldehyde using the procedure similar to that from [47]. The membrane was then placed in a water bath at 37°C in a 2.5% GA solution in 0.01 M phosphate-buffered saline (pH $\approx$ 8.0) for 90 min. After each processing step, the track membrane samples were washed with deionized water. Figure 2

Table 2. Characteristics of track-etched membranes used in the experiment.

No.	Sample designation	Pore diameter by SEM, μm	Pore density, cm^{-2}	Thickness, μm
1	TM-0.1	0.10	$1.0 \cdot 10^9$	12
2	TM-0.4	0.42	$2.7 \cdot 10^8$	19
3	TM-0.5	0.55	$1.5 \cdot 10^8$	12
4	TM-1.1	1.06	$2.5 \cdot 10^7$	22
5	TM-7.1	7.1	$1.3 \cdot 10^5$	17

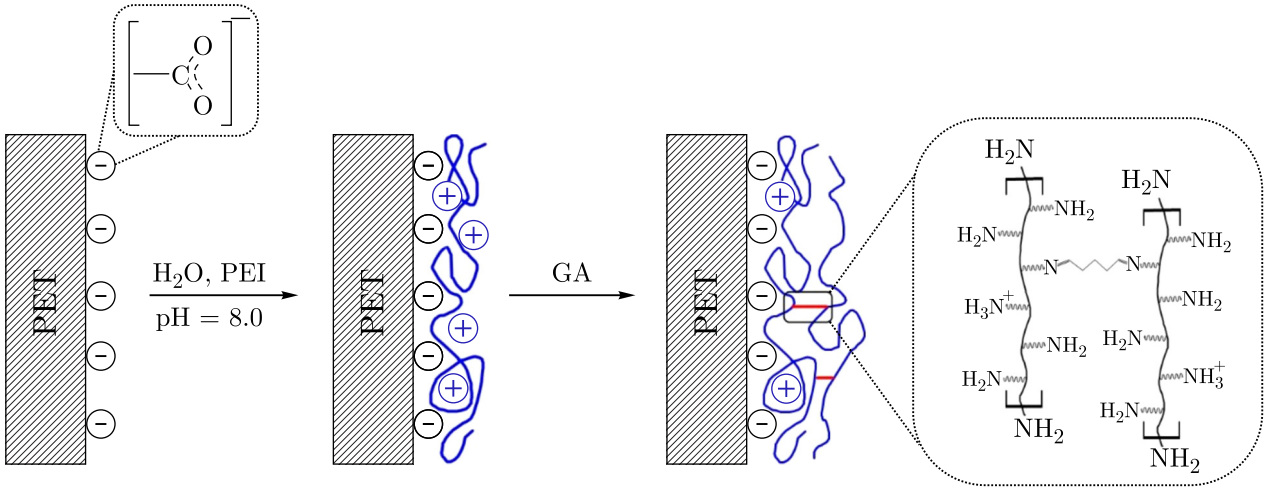

Figure 2. Proposed scheme for membrane modification with polyethyleneimine and subsequent cross-linking with glutaraldehyde.

shows a possible mechanism for the membrane modification. These membranes will henceforth be referred to as TMs.

At pH $\approx$ 7.0, the original TMs had a ζ-potential of –35 mV. After modification with PEI, the track membrane surface was recharged, resulting in the ζ-potential of +34 mV. Cross-linking with GA did not significantly change the ζ-potential, which measured +36 mV. The positive surface charge within the pH range of 6.0–7.0 ensured the electrostatic attraction of silver NPs from the colloidal solution, at pH of 6.8.

3.3. Synthesis of colloidal silver nanoparticles

A colloidal solution of silver NPs was obtained by an electric discharge between two silver electrodes immersed in distilled water. The technique is detailed in [18]. The specific electrical conductivity of the colloidal solution was $\sim$ 20 μS/cm. The average diameter of silver NPs, according to transmission electron microscopy (TEM), was 24 nm, with the root-mean-square deviation of 14 nm (Figure 3).

According to atomic emission spectrometry, the total silver content in the resulting colloidal solution was 4 mg/l. The concentration of NPs, calculated using the average cubic diameter, $\langle d^3_{\mathrm{NP}} \rangle^{1/3} = 32$ nm, was found to be $2 \cdot 10^{10}$ pcs/mL. The ζ-potential of the silver nanoparticle surface measured –25.6 mV.

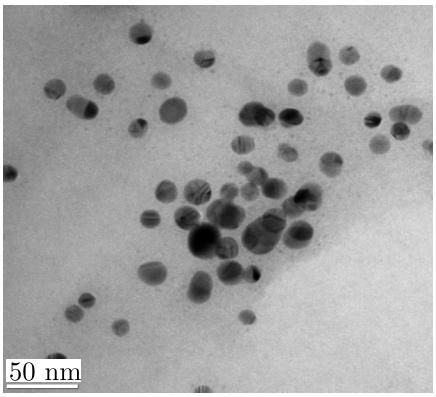

Figure 3. TEM micrograph of silver NPs.

3.4. Filtration of a colloidal solution of silver nanoparticles

Prepared membrane samples were placed in a Millipore filtration cell with an effective diameter of 4.0 cm, and 50 ml of the solution was filtered. The applied pressure varied from (0.020 ± 0.003) to (2.0 ± 0.1) bar. The height of the liquid column determined the lowest pressure, while higher differential pressures were achieved using compressed nitrogen.

3.5. Experimental methods

The silver nanoparticle retention efficiency by TMs was determined using optical absorption spectroscopy. The localized surface plasmon resonance (LSPR) peak at 400 nm, characteristic of silver NPs, was employed as analytical signal. The absorption spectra in the ultraviolet and visible regions were obtained using an Evolution 600 dual-beam spectrophotometer (Thermo Scientific). The instrument was set with a spectral slit width of 2 nm, a scanning step of 1 nm, and a scanning speed of 240 nm/min. The solutions were analyzed in a quartz cuvette with a 1 cm optical path length. Measurements were performed before and after filtration of the colloidal solution through TMs, and the LSPR peak intensities were compared.

The ζ-potential of NPs was measured using a Zetasizer Nano ZSP (Malvern) in a U-shaped cuvette with gold electrodes. The nanoparticle size distribution was characterized using TEM (Talos F200iS/TEM (Thermo Scientific)) at an accelerating voltage of 200 kV. Supplies (SPI) copper grids with an amorphous carbon film were used as the substrate. The nanoparticle sizes and their standard deviations were determined from micrographs using JMicroVision 1.3.4.

The total silver content of the colloidal solution was determined using an EXPEC-6000 inductively coupled plasma atomic emission spectrometer (Focused Photonics Inc.).

The membrane surface charge was determined by measuring the streaming potential. The track membrane samples with a diameter of 2.5 cm were placed in a cell with silver chloride electrodes. The potential difference was measured as a function of pressure within the range of 0.2–1.0 bar, while passing a 0.01 M KCl solution at pH of 6.0. The potential difference was measured using a B7-78/1 digital voltmeter with a sensitivity of 1 μV.

Field-emission scanning electron microscopy (SEM) was performed using a SU 8020 microscope (Hitachi) at an accelerating voltage of 3 kV with a secondary electron detector. A conductive Pt–Pd layer with a thickness of 5 nm was deposited on the samples using magnetron sputtering on a Q-150T S instrument (Quorum).

The content of silver in TMs was determined using a Hitachi S-3400N scanning electron microscope equipped with an energy-dispersive X-ray analysis system at an accelerating voltage of 20 kV. A layer of carbon $\sim$ 15 nm thick was applied to the test samples using a Supplies

Vacu Prep II (SPI) system. Measurements were taken at four points on each sample, the values were averaged, and the standard deviation was calculated.

4. Results and discussion

4.1. Efficiency of silver nanoparticle retention

Based on the proposed theoretical model, TMs with minimum (0.1 μm) and maximum (7.1 μm) diameters were considered first. For TM-0.1, the $\mathfrak{p}$-criterion is much smaller than 1 (Table 1), indicating the possibility of complete silver nanoparticle retention on TMs during filtration. It was observed that nearly 100% particle retention occurs during filtration at pressures ranging from 0.02 to 2.0 bar. In contrast, for TM-7.1, the $\mathfrak{p}$-criterion $\geqslant 1$ (Table 1), suggesting a low probability of nanoparticle retention on these TMs. Experiments showed that at a pressure drop of 0.02 bar on the TM-7.1 sample, the retention percentage was about 5%. Due to the measurement limitations with lower retention values, further experiments across the entire pressure range for this membrane were deemed unreasonable.

The proposed filtration model was also tested using TM-0.4, TM-0.5, and TM-1.1 membranes, for which $\mathfrak{p}$ is on the order of 1 (Table 1). Therefore, the retention of NPs was anticipated to depend on the applied pressure.

Figure 4 presents the efficiency of silver nanoparticle retention as a function of the pressure drop and as a function of the $\mathfrak{p}$-criterion.

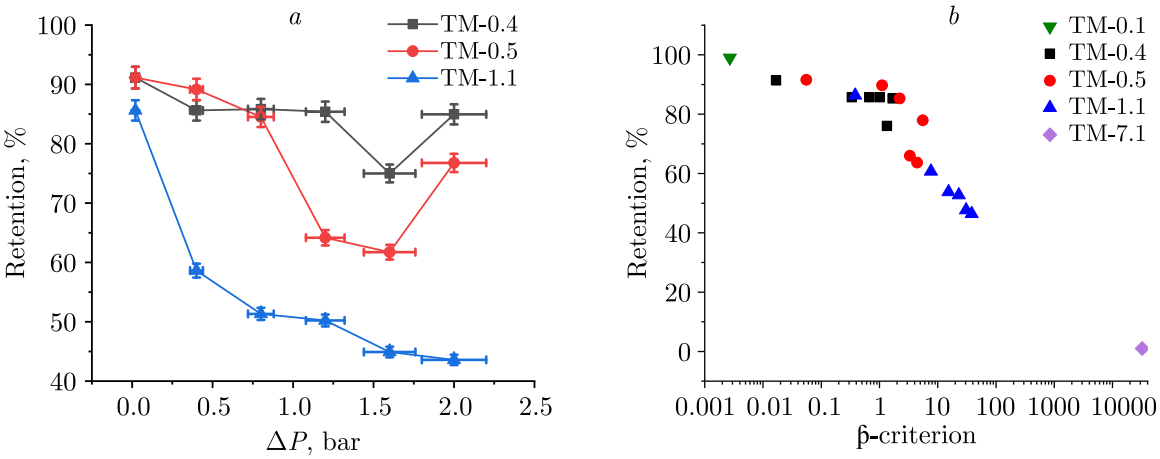

Figure 4. The efficiency of silver nanoparticle retention, calculated from the change in the LSPR peak intensity in the solution after filtration through TMs, as a function of the pressure drop (*a*) and the $\mathfrak{p}$-criterion (*b*).

Figure 4, *a* shows a decrease in silver nanoparticle retention efficiency with increasing pressure for all the TMs considered. This observation aligns with the filtration model discussed earlier. As pressure increases, the flow rate increases, reducing the interaction time between silver NPs and TMs.

Figure 4, *b* depicts how the silver nanoparticle retention efficiency is influenced by the $\mathfrak{p}$-criterion, which considers both the applied pressure and the structural parameters of the membrane (such as pore radius and thickness). The set of points for all TMs forms a single group. Notably, nearly complete retention of silver NPs occurs when $\mathfrak{p} \ll 1$. A transition region is

observed for $\mathfrak{p} \approx 1$, whereas for $\mathfrak{p} \gg 1$, silver NPs pass through TMs. Overall, there is a clear trend of decreasing retention efficiency as the $\mathfrak{p}$-criterion increases.

Furthermore, energy-dispersive X-ray analysis was performed to determine the silver content on TMs after filtration of the silver colloidal solution (Figure 5).

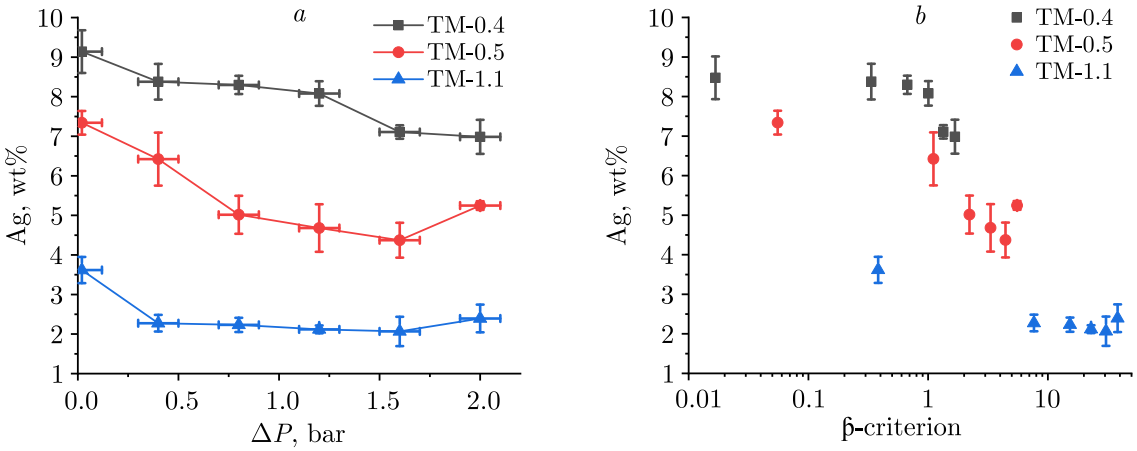

Figure 5. Silver content in wt% on the front surface of the track membrane as a function of pressure drop (*a*) and the $\mathfrak{p}$-criterion (*b*).

Figure 5, *a* shows a noticeable decrease in silver content on TMs as the applied pressure increases (i.e. with increasing colloidal solution flow rate). The relationship between silver content on TMs and the $\mathfrak{p}$-criterion is presented in Figure 5, *b*. In Figure 5, *b*, the experimental data points cluster into three groups, each corresponding to one of the three membranes. At the same values of the $\mathfrak{p}$-criterion, the data points related for different TMs are spaced apart. This spacing occurs because energy dispersive X-ray analysis reflects the silver content only on the front surface of the track membrane, while the $\mathfrak{p}$-criterion considers retention across the entire surface, including pores. For this reason, the graph does not show a clear pattern, although a general trend toward decreasing silver content with increasing $\mathfrak{p}$-criterion is evident.

Figures 4, *a* and 5, *a* reveal anomalies in particle retention and capture by membrane surface at a pressure of 2.0 bar, which the proposed model does not predict. One possible explanation is the inertia of the particles, which might increase the efficiency of their retention. The influence of the particle inertial deposition mechanism can be characterized using the Stokes number St, calculated using the equation [48]:

$$St = \frac{C d_{\text{NP}}^2 \rho_p v_{\text{pore}}}{9\mu 2r}, \tag{6}$$

where ρ_p — gravimetric density of nanoparticles, C — Cunningham slip correction factor (for liquids equal to 1), d_{NP} — diameter of nanoparticles, r — pore radius, v_{pore} — flow rate of the nanoparticle solution in the pore. The calculated values of St at pressures of 0.02–2.0 bar for all TMs fall between $2 \cdot 10^{-7}$ and $3 \cdot 10^{-4}$, that is, much less than 1. This indicates that the inertial mechanism in the system under consideration does not contribute to the efficiency of silver nanoparticle retention.

Another possible explanation for the increased particle retention at 2.0 bar is the recharging of the membrane surface near the pore entrance [41, 42]. The measured value of streaming potential at the beginning of filtration at a pressure of 2.0 bar was +0.15 mV, corresponding

to a positively charged membrane. At the end of filtration, the streaming potential decreased down to –0.012 mV, indicating membrane recharging. This recharging occurs due to the high surface concentration of captured NPs at the pore edges generating an electric field that hinders the passage of particles into the pore channel. This effect may promote the deposition of such particles on the remaining positively charged areas of the track membrane front surface.

4.2. Distribution of silver NPs on the track membrane surface

Stable nanoparticle suspensions were deliberately used in this study to prevent undesirable effects of coagulation. The absence of coagulation was assessed from absorption spectra of solutions before and after filtration (the spectra are provided in the Supplementary Materials, figs. S1 and S2). A slight red shift in the peak position was observed, which may indicate that smaller particles are captured by the membrane with a higher probability. The smaller the pore size, the more pronounced is the shift. At the same time, no increase in background was observed, indicating the absence of coagulation.

Using SEM, micrographs of the track membrane front surface with deposited NPs were obtained. Sectors with vertices at the center of the pores were imposed in the images (Figure 6). The orientation of each sector was chosen such that no other pores were nearby. The sector angle was set to 30°. Circles with radii R_i divided the sector into annular sectors, and within each of these sectors, the number of particles N was counted.

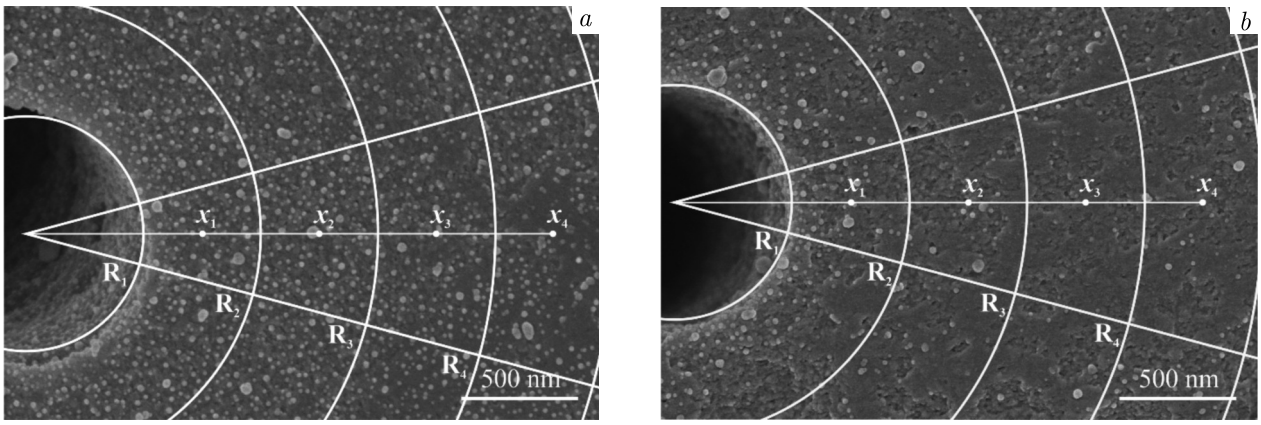

Figure 6. Micrographs of TM-1.1 with precipitated nanoparticle filtration at a pressure of 0.02 bar (*a*) and of 2.0 bar (*b*).

The area of each annular sector was calculated using the following formula:

$$S_i = \pi \frac{\varphi}{360^\circ}(R_{i+1}^2 - R_i^2), \tag{7}$$

where R_i — radius of the i-th circle, R_{i+1} — radius of the next circle, φ — sector angle. The radius of the first circle is equal to the pore radius, $R_1 = r$.

The distance from the center of the pore to the center of the annular sector x_i was calculated using the formula (7):

$$x_i = r\left(i + \frac{1}{2}\right). \tag{8}$$

The particle surface density n was calculated as the ratio of the number N of particles to the area of an annular sector.

The distribution pattern of the nanoparticle depends on the applied pressure. At low pressures, the particles are distributed more uniformly over the track membrane surface. However, at higher pressures, the particles tend to localize at the pore entrance. It is noteworthy that NPs are observed also within the pores. These patterns of nanoparticle distribution support the proposed simple model.

The calculated values of the silver nanoparticle surface density on the membranes front side are presented as a function of the distance from the pore center to the middle of the annular sector (Figure 7). Experimental data points are plotted along the abscissa axis with a step equal to the width of the annular sector (horizontal error bars). Vertical error bars indicate the relative statistical error of the particle counting ($\sqrt{N}/N$).

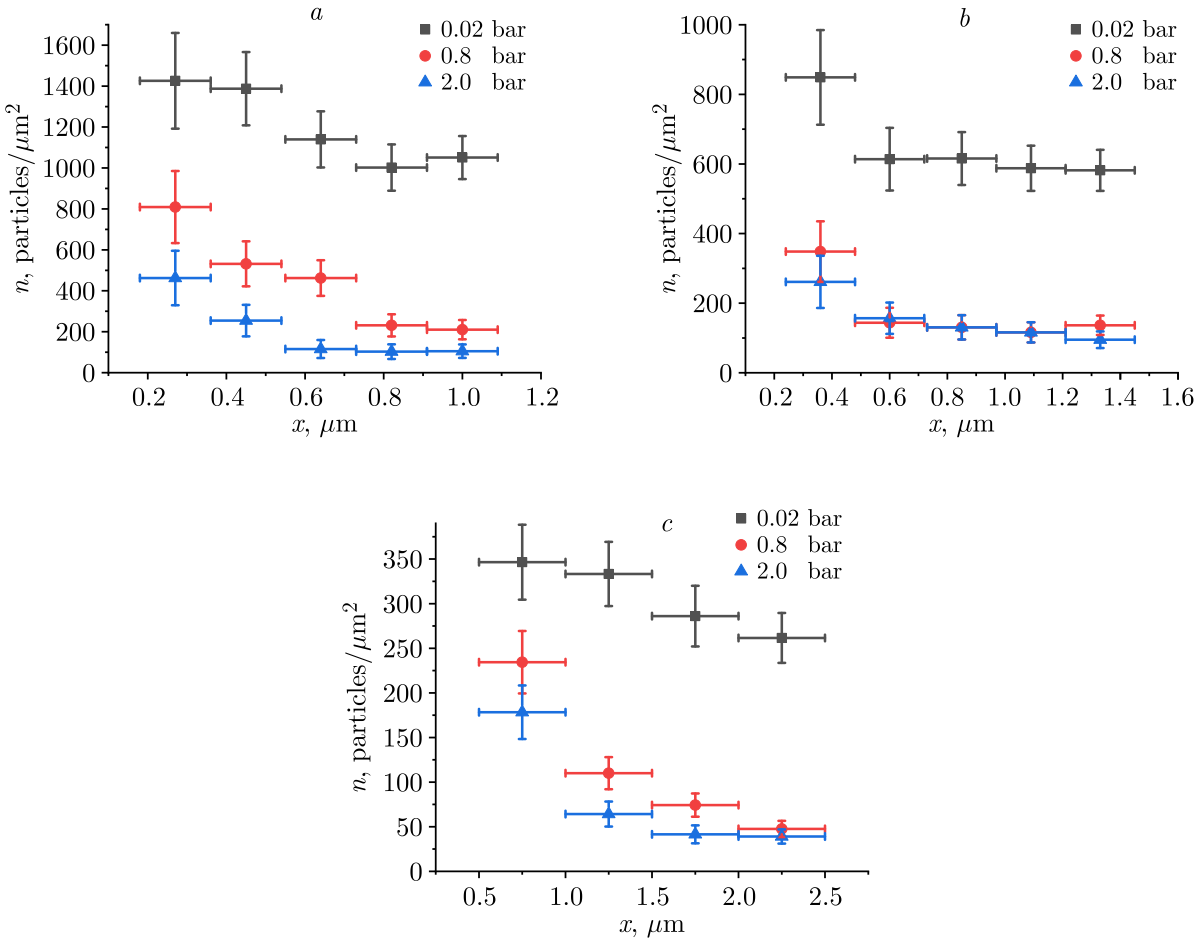

Figure 7. Silver nanoparticle surface density on the membranes TM-0.4 (*a*), TM-0.5 (*b*), TM-1.1 (*c*) as a function of distance from the pore center. Filtration at pressures of 0.02, 0.8, 2.0 bar.

The graphs in Figure 7 show a noticeable decrease in the particle surface density for all samples as the distance from the pore increases. Additionally, higher pressure during filtration leads to a decrease in the average surface density of NPs on the front side of the track membrane. This allows predictions of the density of NPs filling the track membrane surface and whether a gradient or uniform coating will be achieved.

The properties of the resulting nanostructures can be controlled by varying the flow rate and structural parameters of TMs. For example, to achieve a dense and uniform coverage of the membrane surface with NPs, it is advisable to select a membrane with a smaller pore

diameter and greater thickness. These filtration conditions correspond to a ϐ-criterion value of < 1. Conversely, to localize NPs near the pore entrance, a thinner membrane should be used and filtration conducted at a higher pressure, resulting in higher ϐ-criterion values.

4.3. Applicability of the model

As seen in Figure 5, *b*, the dependence of retention on the ϐ-criterion is not steep. Instead, the retention changes gradually across a wide range of ϐ values. Several factors contribute to the slow decrease in retention as ϐ increases. The characteristic time of diffusion τ_D in expression (2) corresponds to a mean distance r which is the center of a Gaussian distribution (probability vs. radius). Therefore, a considerable fraction of particles do not reach the pore wall by the time τ_D occurs. Additionally, NPs are not monodisperse and exhibit a range of diffusion coefficients. Furthermore, there is a parabolic velocity profile in the pore channels, with the average flow velocity v_{pore} equal to half the maximum velocity at the channel centerline ($r = 0$). Particles entering the pore in the vicinity of the centerline pass through the channel faster and have a lower probability to be captured by walls. All these complexities indicate that a more sophisticated theory is needed to describe this scenario fully. In the future, to refine the theory and fully resolve the nanoscale distribution of immobilized nanoparticles — particularly their three-dimensional localization on membrane surface and within pore channels — it seems feasible to apply the recently developed methods of 3D superresolution optical nanoscopy [49]. Nevertheless, our experiments showed clear correlation between total retention and τ_D/τ_m values, suggesting that the proposed formalism can be used as a simple predictive model.

This study primarily aimed to optimize the immobilization of noble metal NPs for the fabrication of sensors based on the SERS effect. The established patterns allow for control and prediction of the average concentration and uniformity of nanoparticle distribution on the active surface of the membrane sensor. When using the membrane sensor in flow-through mode, the proposed retention criterion would be useful for selecting the pore diameter and filtration mode to adsorb the maximum amount of analyte with the desired localization on the porous substrate.

It should be noted that the conditions for the applicability of the proposed model include low concentrations of colloidal solutions and suspensions, as well as pore sizes significantly larger than the nanoparticle sizes. Due to the latter, we neglected possible steric hindrance effects on particle retention [50]. The model is not applicable when a precipitate layer may form on the membrane ("cake filtration"). The fabrication of SERS-based sensors does not require the accumulation of more than one monolayer of NPs. This principle determined the experimental conditions in this study, namely, the relationship between the amount of solution, its concentration, particle size, and membrane area. In this study, the membranes operational mode was controlled by the pressure drop across it. An alternative approach could involve controlling the flow rate as the key parameter [51]. In this case, the τ_D/τ_m ratio can be managed more accurately.

The proposed model can also be used to the application of biological entities, such as viruses, cancer cells [52–54], DNA-binding proteins [55], and other components to ensure affinity filtration [51], onto the surface of a membrane.

5. Conclusion

This paper proposes a method for controlled deposition of nanoparticles onto the surface of a track-etched membrane via filtration of a colloidal solution. A straightforward model is

developed to predict nanoparticle retention efficiency by accounting for convective and diffusive transport within the membrane pores. The model was experimentally validated using a colloidal solution of silver NPs with an average diameter of 24 nm and track-etched membranes with various structural parameters.

The surfaces of both the membrane and the nanoparticles had opposite electrical charges. The results demonstrate that the concentration of particles on the membrane surface is influenced by the ratio of the volume of the solution passed to the membrane area, as well as a dimensionless criterion that incorporates factors such as pore radius, membrane thickness, viscosity of the medium, diffusion coefficient of NPs, and pressure drop.

Moreover, the study shows that the average concentration of immobilized particles and their distribution on the membrane surface can be controlled by adjusting the flow rate. This developed approach has the potential to be extended to other porous substrates and different types of nanoparticles for depositing controlled amounts of substances. This technique can aid in creating composite materials with desired properties.

The findings highlight the potential for integrating functional nanocomposite sensor systems with flow-through designs, which could significantly advance the development of analytical and biosensors.

Acknowledgements

The authors are grateful to Alisher Mutali (FLNR JINR) for the help with TEM examination of samples.

Author contributions

I. Fadeikina: Writing, Original draft preparation, Investigation, Validation, Reviewing and Editing; E. Andreev: Reviewing and Editing, Writing, Original draft preparation, Visualization, Investigation; O. Kristavchuk: Data curation, Investigation; O. Orelovich: Investigation, Visualization; P. Apel: Conceptualization, Methodology, Supervision, Validation.

Funding

The research was funded by the Joint Institute for Nuclear Research within the framework of projects “Nanocomposite and Functional Track Membranes” 07-5-1131-2-2024/2028.

Conflicts of interest

The authors declare no conflicts of interest.

References

[1] J. Kim, The use of nanoparticles in polymeric and ceramic membrane structures: Review of manufacturing procedures and performance improvement for water treatment, Environ. Pollut. 158 (7) (2010) 2335–2349. https://doi.org/10.1016/j.envpol.2010.03.024.

[2] M. Ulbricht, Advanced functional polymer membranes, Polymer 47 (7) (2006) 2217–2262. https://doi.org/10.1016/j.polymer.2006.01.084.

[3] A. B. Yaroslavtsev, Y. A. Dobrovolsky, L. A. Frolova, E. V. Gerasimova, E. A. Sanginov, N. S. Shaglaeva, Nanostructured materials for low-temperature fuel cells, Russ. Chem. Rev. 81 (3) (2012) 191–220. https://doi.org/10.1070/RC2012v081n03ABEH004290.

[4] Yu. A. Krutyakov, A. A. Kudrinskiy, A. Yu. Olenin, G. V. Lisichkin, Synthesis and properties of silver nanoparticles: Advances and prospects, Russ. Chem. Rev. 77 (3) (2008) 233–257. https://doi.org/10.1070/RC2008v077n03ABEH003751.

[5] D. D. Evanoff, G. Chumanov, Synthesis and optical properties of silver nanoparticles and arrays, ChemPhysChem 6 (7) (2005) 1221–1231. https://doi.org/10.1002/cphc.200500113.

[6] J. S. Taurozzi, V. V. Tarabara, Silver nanoparticle arrays on track etch membrane support as flow-through optical sensors for water quality control, Environ. Engin. Sci. 24 (1) (2007) 122–137. https://doi.org/10.1089/ees.2007.24.122.

[7] A. Yu. Solov'ev, T. S. Potekhina, I. A. Chernova, B. Ya. Basin, Track membrane with immobilized colloid silver particles, Russ. J. Appl. Chem. 80 (3) (2007) 438–442.

[8] O. V. Kristavchuk, I. V. Nikiforov, A. N. Nechaev, P. Y. Apel, V. I. Kukushkin, Immobilization of silver nanoparticles obtained by electric discharge method on a track membrane surface, Colloid J. 79 (5) (2017) 637–646. https://doi.org/10.7868/S0023291217050093.

[9] B. Krafft, R. Panneerselvam, D. Geissler, D. Belder, A microfluidic device enabling surface-enhanced Raman spectroscopy at chip-integrated multifunctional nanoporous membranes, Anal. Bioanal. Chem. 412 (2020) 267–277. https://doi.org/10.1007/s00216-019-02228-9.

[10] R. L. Fleischer, P. B. Price, R. M. Walker, Nuclear Tracks in Solids, California Press, Berkeley, 1973.

[11] D. M. Karl, Plastics-irradiated-etched: The Nuclepore filter turns 45 years old, Limnol. Oceanogr. Bull. 16 (2007) 49–54. https://doi.org/10.1002/iroh.200711044.

[12] P. Y. Apel, Track-Etching, in: Encycl. Membr. Sci. Technol., John Wiley & Sons. Inc., Hoboken, NJ, USA, 2013, pp. 1–25. https://doi.org/10.1002/9781118522318.emst040.

[13] P. Y. Apel, Fabrication of functional micro- and nanoporous materials from polymers modified by swift heavy ions, Radiat. Phys. Chem. 159 (2019) 25–34. https://doi.org/10.1016/j.radphyschem.2019.01.009.

[14] A. Kros, R. J. M. Nolte, N. A. J. M. Sommerdijk, Conducting polymers with confined dimensions: Track-etch membranes for amperometric biosensor applications, Adv. Mater. 14 (2002) 1779–1782. https://doi.org/10.1002/1521-4095(20021203)14:23<1779::AID-ADMA1779>3.0.CO;2-T.

[15] B. Schiedt, K. Healy, A. P. Morrison, R. Neumann, Z. Siwy, Transport of ions and biomolecules through single asymmetric nanopores in polymer films, Nucl. Instrum. Meth. Phys. Res. B 236 (2005) 109–116. https://doi.org/10.1016/j.nimb.2005.03.265.

[16] L. T. Sexton, L. P. Horne, S. A. Sherrill, G. W. Bishop, L. A. Baker, C. R. Martin, Resistive-pulse studies of proteins and protein/antibody complexes using a conical nanotube sensor, J. Am. Chem. Soc. 129 (2007) 13144–13152. https://doi.org/10.1021/ja0739943.

[17] P. Y. Apel, I. V. Blonskaya, S. Dmitriev, O. L. Orelovitch, A. Presz, B. A. Sartowska, Fabrication of nanopores in polymer foils with surfactant-controlled longitudinal profile, Nanotechnology 18 (2007) 305302. https://doi.org/10.1088/0957-4484/18/30/305302.

[18] O. V. Kristavchuk, A. S. Sohatsky, V. V. Skoi, A. I. Kuklin, V. V. Trofimov, A. N. Nechaev, P. Y. Apel', V. I. Kozlovskiy, V. V. Sleptsov, Structural characteristics and ionic composition of a colloidal solution of silver nanoparticles obtained by electrical-spark discharge in water, Colloid J. 83 (4) (2021) 448–460. https://doi.org/10.31857/S0023291221040042.

[19] V. R. Oganesyan, O. L. Orelovich, I. V. Yanina, P. Yu. Apel', Study of retention ability of nucleopore membranes, Colloid J. 63 (6) (2001) 755–761.

[20] A. O. Orlova, Yu. A. Gromova, A. V. Savelyeva, V. G. Maslov, M. V. Artemyev, A. Prudnikau, A. V. Fedorov, A. V. Baranov, Track membranes with embedded semiconductor nanocrystals: Structural and optical examinations, Nanotechnology 22 (2011) 455201. https://doi.org/10.1088/0957-4484/22/45/455201.

[21] T. Y. Ling, J. Wang, D. Y. H. Pui, Measurement of filtration efficiency of Nuclepore filters challenged with polystyrene latex nanoparticles: Experiments and modeling, J. Nanopart. Res.

13 (2011) 5415–5424. https://doi.org/10.1007/s11051-011-0529-2.

[22] A. Duek, E. Arkhangelsky, R. Krush, A. Brenner, V. Gitis, New and conventional pore size tests in virus-removing membranes, Water Res. 46 (8) (2012) 2505–2514. https://doi.org/10.1016/j.memsci.2021.119417.

[23] S.-C. Chen, D. Segets, T.-Y. Ling, W. Peukert, D. Y. H. Pui, An experimental study of ultrafiltration for sub-10 nm quantum dots and sub-150 nm nanoparticles through PTFE membrane and Nuclepore filters, J. Membr. Sci. 497 (2016) 153–161. https://doi.org/10.1016/j.memsci.2015.09.022.

[24] H. Lee, D. Segets, S. Süß, W. Peukert, S.-C. Chen, D. Y. H. Pui, Liquid filtration of nanoparticles through track-etched membrane filters under unfavorable and different strength conditions: Experiments and modeling, J. Membr. Sci. 524 (2017) 682–690. https://doi.org/10.1016/j.memsci.2016.11.023.

[25] I. Kulik, Yu. Eremchev, P. Yu. Apel, D. L. Zagorski, A. V. Naumov, Fluorescence imaging of ultrafiltration of single nanoparticles from colloid solution in track membranes, J. Appl. Spectrosc. 85 (5) (2018) 814–821.

[26] A. Delavari, D. Breite, A. Schulze, R. E. Baltus, Latex particle rejection from virgin and mixed charged surface polycarbonate track etched membranes, J. Membr. Sci. 584 (2019) 110–119. https://doi.org/10.1016/j.memsci.2019.04.065.

[27] H. Lee, D. Segets, S. Süß, W. Peukert, S.-C. Chen, D. Y. H. Pui, Effects of filter structure, flow velocity, particle concentration and fouling on the retention efficiency of ultrafiltration for sub-20 nm gold nanoparticles, Sep. Purif. Technol. 241 (2020) 116689. https://doi.org/10.1016/j.seppur.2020.116689.

[28] S. Y. Liu, Z. Chen, P. Sanaei, Effects of particles diffusion on membrane filters performance, Fluids 5 (2020) 121. https://doi.org/10.3390/fluids5030121.

[29] H. Urch, C. Geisman, M. Ulbricht, M. Epple, Deposition of functionalized calcium phosphate nanoparticles on functionalized polymer surface, Mat.-wiss. u. Werkstofftech 37 (6) (2006) 422–425. https://doi.org/10.1002/mawe.200600008.

[30] M. Elimelech, Particle deposition on ideal collectors from dilute flowing suspensions: Mathematical formulation, numerical solution, and simulations, Sep. Technol. 4 (1994) 186–212. https://doi.org/10.1016/0956-9618(94)80024-3.

[31] Sh. Yamamoto, H. Koshikawa, T. Taguchi, T. Yamaki, Precipitation of Pt nanoparticles inside ion-track-etched capillaries, Quantum Beam Sci. 4 (2020) 8. https://doi.org/10.3390/qubs4010008.

[32] J.-N. Kao, Y. Wang, R. Pfeffer, S. Weinbaum, A theoretical model for Nuclepore filters including hydrodynamic and molecular wall interaction effects, J. Colloid Interface Sci. 121 (1988) 543–557.

[33] V. I. Kukushkin, A. B. Van'kov, I. V. Kukushkin, Long-range manifestation of surface-enhanced Raman scattering, JETP Lett. 98 (2) (2013) 64–69. https://doi.org/10.1134/S0021364013150113.

[34] V. Shvalya, G. Filipic, J. Zavasnik, I. Abdulhalim, U. Cvelbar, Surface-enhanced Raman spectroscopy for chemical and biological sensing using nanoplasmonics: The relevance of interparticle spacing and surface morphology, Appl. Phys. Rev. 7 (2020) 031307. https://doi.org/10.1063/5.0015246.

[35] W. R. Bowen, J. I. Calvo, A. Hernández, Steps of membrane blocking in flux decline during protein microfiltration, J. Membr. Sci. 101 (1–2) (1995) 153–165. https://doi.org/10.1016/0376-7388(94)00295-A.

[36] C.-C. Ho, A. L. Zydney, A combined pore blockage and cake filtration model for protein fouling during microfiltration, J. Colloid Interface Sci. 232 (2) (2000) 389–399. https://doi.org/10.1006/jcis.2000.7231.

[37] P. Y. Apel, S. Velizarov, A. V. Volkov, A. B. Yaroslavtsev, T. V. Eliseeva, A. V. Parshina, V. V. Ni-

konenko, N. D. Pismenskaya, K. I. Popov, Fouling and membrane degradation in electromembrane and baromembrane processes, Membranes and Membrane Technol. 4 (2) (2022) 69–92. https://doi.org/10.1134/S2218117222020031.

[38] C. Duclos-Orsello, W. Li, C.-C. Ho, A three mechanism model to describe fouling of microfiltration membranes, J. Membr. Sci. 280 (1–2) (2006) 856–866. https://doi.org/10.1016/j.memsci.2006.03.005.

[39] J. Lin, D. Bourrier, M. Dilhan, P. Duru, Particle deposition onto a microsieve, Phys. Fluids 21 (2009) 073301. https://doi.org/10.1007/s11242-022-01810-7.

[40] G. C. Agbangla, E. Climent, P. Bacchin, Experimental investigation of pore clogging by microparticles: Evidence for a critical flux density of particle yielding arches and deposits, Sep. Purif. Technol. 101 (2012) 42–48. https://doi.org/10.1016/j.seppur.2012.09.011.

[41] W. R. Bowen, A. N. Filippov, A. O. Sharif, V. M. Starov, A model of the interaction between a charged particle and a pore in a charged membrane surface, Adv. Colloid Interface Sci. 81 (1999) 35–72. https://doi.org/10.1134/S0965544111070085.

[42] A. N. Filippov, T. S. Philippova, Electrostatic and molecular interaction between a charged spherical particle and a charged membrane pore: The case of given surface charge densities? Membranes and Membrane Technol. 3 (1) (2021) 15–23. https://doi.org/10.1134/S2218117221010065.

[43] J. Happel, H. Brenner, Low Reynolds Number Hydrodynamics, Mir, Moscow, 1976, p. 630.

[44] J. I. Calvo, A. Hernandez, P. Pradanos, F. Tejerina, Charge adsorption and zeta potential in cyclopore membranes, J. Colloid Interface Sci. 181 (1996) 399–412. https://doi.org/10.1006/jcis.1996.0397.

[45] E. Z. Gribova, A. I. Saichev, Fizicheskij podkhod k analizu diffuzii chastits: Monografiya, Izd-vo Nizhegorodskogo gosuniversiteta, Nizhnij Novgorod, 2012, p. 232 (In Russian).

[46] V. M. Sukhov, O. V. Dement'eva, M. E. Kartseva, V. M. Rudoy, V. A. Ogarev, Metal nanoparticles on polymer surfaces: 3. Adsorption kinetics of gold hydrosol particles on polystyrene and poly(2-vinylpyridine), Colloid J. 66 (4) (2004) 482–488. https://doi.org/10.1134/S1061933X1606003X.

[47] A. Movahedi, A. Lundin, N. Kann, M. Nydén, K. Moth-Poulsen, Cu(I) stabilizing crosslinked polyethyleneimine, Phys. Chem. Chem. Phys. 17 (2015) 18327–36. https://doi.org/10.1039/c5cp02198g.

[48] K. L. Rubow, B. Y. H. Liu, Characteristics of Membrane Filters for Particle Collection, in: Raber R.R. (Ed.), Fluid Filtration: Gas, Vol. 1, ASTM STP 975, American Society for Testing and Materials, Philidelphia, 1986.

[49] I. Yu. Eremchev, M. Yu. Eremchev, A. V. Naumov, Multifunctional far-field luminescence nanoscope for studying single molecules and quantum dots (50th anniversary of the Institute of Spectroscopy, Russian Academy of Sciences), Phys. Usp. 62 (3) (2019) 294–303. https://doi.org/10.3367/UFNe.2018.06.038461.

[50] R. E. Beck, J. S. Schultz, Hindrance of solute diffusion within membranes as measured with microporous membranes of known pore geometry, Biochim. Biophys. Acta 255 (1972) 273–303.

[51] C. Cockerham, A. Caruthers, J. McCloud, L. M. Fortner, S. Youn, S. P. McBride, Azo-dye-functionalized polycarbonate membranes for textile dye and nitrate ion removal, Micromachines 13 (2022) 577. https://doi.org/10.3390/mi13040577.

[52] E. S. Peri Ibàñez, M. H. Argüelles, C. Y. Flores, M. G. Mandile, M. C. Carzoglio, Design and development of a syringe-based POCT prototype using track-etched PET membranes for simple and rapid detection of group A Rotavirus in human samples, ACS Infectious Diseases 11 (8) (2025) 2205–2217. https://doi.org/10.1021/acsinfecdis.5c00239.

[53] V. Kukushkin, O. Kristavchuk, E. Andreev, N. Meshcheryakova, O. Zaborova, A. Gambaryan, A. Nechaev, E. Zavyalova, Aptamer-coated track-etched membranes with a nanostructured silver layer for single virus detection in biological fluids, Front. Bioengin. Biotechnol. 10 (2023) 1076749. https://doi.org/10.3389/fbioe.2022.1076749.

[54] M. Zinggeler, T. Brandstetter, J. Rühe, Biophysical insights on the enrichment of cancer cells from whole blood by (affinity) filtration, Sci. Rep. 9 (1) (2019) 1246. https://doi.org/10.1038/s41598-018-37541-3.

[55] M. Zarubin, E. Andreev, E. Kravchenko, U. Pinaeva, A. Nechaev, P. Apel, Developing tardigrade-inspired material: Track membranes functionalized with Dsup protein for cell-free DNA isolation, Biotechnol. Progr. 40 (5) (2024) e3478. https://doi.org/10.1002/btpr.3478.